Cobalt–Samarium Oxide Composite as a Novel High-Performance Catalyst for Partial Oxidation and Dry Reforming of Methane into Synthesis Gas

A. S. Loktev[a,b,*], V. A. Arkhipova[b], M. A. Bykov[c], A. A. Sadovnikov[a], and A. G. Dedov[a,b]

[a] Topchiev Institute of Petrochemical Synthesis, Russian Academy of Sciences, Moscow, 119991 Russia
[b] Gubkin Russian State University of Oil and Gas (National Research University), Moscow, 119991 Russia
[c] Faculty of Chemistry, Lomonosov Moscow State University, Moscow, 119991 Russia
*e-mail: al57@rambler.ru; genchem@gubkin.ru

Abstract—The paper describes a novel high-performance catalyst that was developed for partial oxidation of methane (POM) and dry reforming of methane (DRM) into synthesis gas. The catalyst is based on samarium cobaltite dispersed in a samarium oxide matrix. Unlike its known counterparts based on samarium cobaltate, the novel catalyst is resistant to carbonization and contains active sites that exhibit higher syngas productivity.

Keywords: synthesis gas, partial oxidation of methane, dry reforming of methane, samarium cobaltite, samarium oxide

Synthesis gas (syngas, a $CO+H_2$ mixture) is one of the most important intermediates in methane conversion to hydrogen and valuable petrochemicals [1–5]. The high cost of syngas production makes its improvement an urgent problem.

Energy-consuming industrial syngas production based on steam reforming of methane (SRM) is commonly used to synthesize a hydrogen-rich product.

Another well-known syngas production process, partial oxidation of methane (POM), has the advantages of exothermicity and a syngas composition suitable for further processing into valuable petrochemicals.

Syngas production by dry reforming of methane (DRM) is generally considered an effective pathway to dispose of the two major greenhouse gases, namely CO_2 and CH_4 [4–8].

There are also syngas production techniques that simultaneously involve three oxidants such as H_2O, O_2, and CO_2 [9, 10].

Relevant thermodynamic calculations have shown, for all the process designs mentioned above, that high CH_4 conversion and high CO and H_2 selectivity levels (above 90%) are only achievable at temperatures above 800°C [4, 6, 7, 11, 12], and that these performance parameters can reach as high as 100% at 900°C.

The typical drawback of syngas production catalysts is their performance deficiency caused by surface carbonization. Therefore, creation of new carbonization-resistant catalysts has remained a challenging problem.

Nickel-based and cobalt-based complex-oxide catalysts produced from various perovskites and perovskite-like materials have exhibited high performance in POM and DRM processes [4–7, 11–29]. Their performance was shown to be largely associated with the formation of fine-dispersed nickel or cobalt metal phases stabilized by rare-earth (REE) and some other oxides. These oxides, along with metallic components, are able to facilitate the catalytic transformations of substrates.

We previously demonstrated that POM and DRM catalysts can be synthesized even without the prior preparation of a completely single-phase initial material [23, 24]. The catalysts can be produced by evaporating an

aqueous solution of cobalt (or nickel) nitrates and REE nitrates followed by rapid (2–3 h) annealing.

When tested in POM [18, 19] and DRM reactions [25–28], the single-phase $SmCoO_3$ perovskites synthesized by the citrate method or Pechini method have shown relatively low performance. In our previous study, a $SmCoO_3$ material consisting of samarium and cobalt oxides along with a perovskite was synthesized by evaporting nitrate solutions and rapid annealing [24]. In POM, this material achieved a syngas yield of 65–67% (at 750°C) and 95–96% (at 900°C); in DRM, the respective yields reached 48–51% (at 700°C) and 98–100% (at 900°C). After the POM and DRM reactions, the catalyst turned into a composite that contained 23 wt % Co dispersed in samarium oxide.

Like in its similarly formulated counterparts described in the literature, the disadvantage of this catalyst was strong carbonization, potentially threatening to clog the reactor in the long run. A variety of publications have reported that the coking of POM and DRM catalysts can be reduced by diminishing the metal particles in them [3–7, 11–21]. One approach to this end is by lowering the amount of cobalt uniformly distributed in the catalyst matrix.

The purpose of the present study was to synthesize a more carbonization-resistant catalyst that would contain 2 wt % of cobalt dispersed in the samarium oxide matrix, and to test it in POM and DRM reactions.

EXPERIMENTAL

To synthesize the catalyst, we used the following Sigma-Aldrich reagents: samarium(III) nitrate hexahydrate (CAS 13759-83-6); and cobalt(II) nitrate hexahydrate (CAS 10026-22-9).

Weighed samples of $Co(NO_3)_2 \cdot 6H_2O$ and $Sm(NO_3)_3 \cdot 6H_2O$ were dissolved in a minimum of distilled water. The solution was dried and calcined at 500°C for 1.3 h and at 700°C for 2 h. The amounts of the reagents corresponded to 2 wt % of cobalt in the resultant catalyst. The synthesized material was designated as **KtSmCoO**.

The phase composition of the material was identified by X-ray powder diffraction (XRD) on a Rigaku MiniFlex 600 diffractometer (CuK_α radiation, $\lambda = 1.54187$ Å) using the database of the International Center for Diffraction Data (ICDD).

Spent catalysts were subjected to thermogravimetric analysis (TGA) in air in the range of 35–900°C at a heating rate of 10°/min. The TGA data were processed using the NETZSCH Proteus Thermal Analysis software package.

The catalyst particle surfaces were examined by scanning electron microscopy (SEM) on a Carl Zeiss NVision 40 microscope with a magnification up to ×200 000 using SE or InLens secondary electron detectors (accelerating voltage 7 kV) and ESB backscattered electron detectors (accelerating voltage 1 kV). The microscope was equipped with an Oxford Instruments X-MAX 80 mm^2 detector with an accelerating voltage of 1–20 kV to measure the elemental composition of samples by X-ray microanalysis (EDX).

The POM and DRM reactions were carried out in an electrically-heated flow-type quartz reactor (inner diameter 18 mm) with an axial thermocouple pocket (outer diameter 8 mm), where an armored chromel–alumel thermocouple 1 mm in diameter was fitted. The thermocouple tip was located in the middle of the catalyst bed.

The catalysts (0.2 g, 0.5–1 mm particles, 1 mm bed) were placed on a quartz fiber support. For POM, the free reactor volume was filled with quartz chips. The setup was similar to that described in [30]. The catalyst was heated up to 900°C in a flow of hydrogen or CH_4–O_2 or CH_4–CO_2 mixtures undiluted with an inert gas ($CH_4/O_2 = 2$; $CH_4/CO_2 = 1$). All the gases (at least 99.9% pure) were manufactured by the Moscow Gas Processing Plant, Russia. The gas mixture flow rate was 7 or 12 liters per gram catalyst per hour (L g^{-1} h^{-1}) for POM and 15 L g^{-1} h^{-1} for DRM. When the catalyst was heated in hydrogen, the hydrogen flow was stopped to start a nitrogen purge followed by the injection of the reagent gas mixture. The reactor temperature was varied using a programmable temperature controller. At a set temperature point, the products were analyzed, after which the temperature was adjusted to other setpoints without stopping the reagent injection. The gas flow rates at the reactor inlet and outlet were measured by a bubble flow meter.

The feed gas mixtures and products were analyzed by a GC method similar to that described in [30, 31], using *GALS 311* chromatographs equipped with thermal conductivity detectors, with helium as a carrier gas. A 2 m × 5 mm steel column packed with Porapak Q was used at 70°C to detect methane, CO_2, ethylene, and ethane, as well as to determine the total content of hydrogen, oxygen, nitrogen, and CO. A similar column
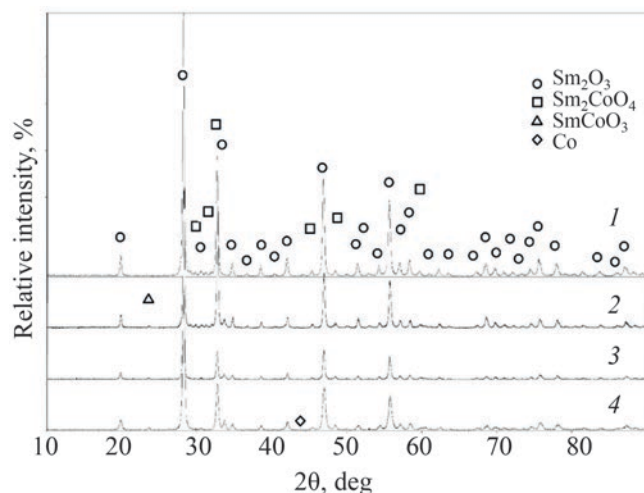
Fig. 1. XRD powder patterns: (*1*) initial **KtSmCoO**; (*2, 3*) post-POM composites; and (*4*) post-DRM composite.

packed with zeolite NaX was used at 30°C to detect hydrogen, oxygen, nitrogen, methane, and CO. The GC data were processed using the *ECOCHROM* hardware/software package.

The methane conversion, $X(CH_4)$ (%), was calculated by the formula:

$$X(CH_4) = \frac{W_{in}(CH_4) - W_{out}(CH_4)}{W_{in}(CH_4)} \times 100,$$

where $W_{in}(CH_4)$ and $W_{out}(CH_4)$ are the moles of methane at the inlet and outlet of the reactor, respectively.

The degrees of oxygen and carbon dioxide conversion, $X(O_2)$ and $X(CO_2)$, were evaluated in a similar manner.

The yield of hydrogen, $Y(H_2)$ (%), was derived by the formula:

$$Y(H_2) = \frac{W_{out}(H_2)}{2W_{in}(CH_4)} \times 100,$$

where $W_{out}(H_2)$ is the moles of hydrogen at the outlet.

The yield of CO, $Y(CO)$ (%), from POM was derived by the formula:

$$Y(CO) = \frac{W_{out}(CO)}{W_{in}(CH_4)} \times 100,$$

where $W_{out}(CO)$ is the moles of CO at the outlet.

The yield of CO_2 from POM was evaluated in a similar manner.

The yield of CO, $Y(CO)$ (%), from DRM was derived by the formula:

$$Y(CO) = \frac{W_{out}(CO)}{W_{in}(CH_4) + W_{in}(CO_2)} \times 100,$$

where $W_{in}(CO_2)$ is the moles of carbon dioxide at the inlet.

In specialized POM and DRM experiments carried out in the reactor with no catalyst loaded, only minor carbonization was observed on the reactor walls, mostly after the quartz packing and quartz fiber layers. Under the DRM conditions, the exhaust gases were found to contain, along with unreacted reagents, trace amounts of CO and hydrogen. In the catalyst-free POM experiment at 900°C, the exhaust gases contained 15% H_2, 25% CO, 7% CO_2, 3% C_2H_4, and 50% CH_4.

RESULTS AND DISCUSSION

Figure 1 provides the XRD patterns both for the initially synthesized **KtSmCoO** (curve *1*) and the spent catalysts after POM (curves *2* and *3*, corresponding to different **KtSmCoO** prereduction conditions as described below) and after DRM (curve *4*).

The XRD data show that the precursor **KtSmCoO** was a cobalt–samarium oxide composite that contained samarium cobaltite (Sm_2CoO_4) and samarium oxide (Sm_2O_3) phases at a weight ratio of 1 : 26 as calculated by the Rietveld method [32]. This corresponds to 0.5 wt % of cobalt, instead of the expected 2 wt %, probably due to the presence of X-ray amorphous cobalt-containing components. At the same time, the EDX data for the samples after POM and DRM (see Figs. 3 and 6) show an average cobalt concentration of about 2 wt %, i.e. the value coinciding with the Co content expected in **KtSmCoO**.

Partial Oxidation of Methane

In the first series of POM experiments with **KtSmCoO**, the catalyst was heated to 900°C in a CH_4–O_2 mixture injected at 7 L g^{-1} h^{-1} (Table 1). At 900°C the yields of CO and H_2 gradually increased, and reached 79% after 5 h (Runs 1 and 2). The prolonged time of the generation of active catalytic sites may be caused both by the hindered access of the reagents to the Co components located inside the Sm_2O_3 particles, and by the increased

Table 1. POM results for KtSmCoO heated to 900°C in CH_4–O_2 mixture

Run no.	Time, min	T, °C	Conversion, %		Yield, %	
			CH_4	O_2	H_2	CO
1	25	900	32	97	5	5
2	320	900	97	96	79	79
3	435	900	99	99	94	94
4	560	850	94	99	77	77
5	635	800	83	99	63	63
6	725	750	29	99	0	0
7	805	900	97	99	93	93

resistance of the Sm_2CoO_4 particles to reduction in the presence of excess Sm_2O_3. As the POM was continued at 900°C (Run 3), the yields of CO and H_2 further rose up to 94%. Subsequent cooling led to a decrease in the yields of CO and H_2, specifically to 77% at 850°C and 63% at 800°C. At 750°C the catalyst became inactive in POM, with only deep oxidation of methane occurring. Nonetheless, both yields regained high levels (93%) after reheating to 900°C.

Thus, Table 1 clearly shows that the composite catalyst generated after POM, with 2 wt % Co in it, provided a high yield of syngas at 800–900°C. The $SmCoO_3$ material that we previously synthesized by a similar technique, contained samarium and cobalt oxides along with a perovskite [24]. The composite with 23 wt % Co generated from the $SmCoO_3$ after POM achieved a syngas yield of 95–96% at 900°C. Despite high performance being

reached immediately, that catalyst was prone to significant surface carbonization to form carbon fibers and nanotubes.

In contrast, the SEM micrographs of the post-POM **KtSmCoO** provide no evidence of significant carbonization in the form of carbon fibers or nanotubes (Fig. 2).

The EDX data for the spent catalyst (Fig. 3) show zero carbon and the average elemental concentrations in the catalyst particles consistent with the composition of the initial material with 2 wt % Co.

The phase composition of the catalyst discharged from the reactor after POM remained unchanged (see curve *1* in Fig. 1). Although metallic cobalt is supposed to be contained in post-POM catalysts based on REE cobaltates [19, 28], the XRD pattern of the spent catalyst actually lacks a metallic cobalt phase. This can be explained by cobalt particle sizes too small to be detected by XRD. In addition, under POM conditions, active cobalt metal particles are able to enter into the reactions of oxidation (1) and subsequent formation of Sm_2CoO_4 (2):

$$3Co + 2O_2 \rightarrow Co_3O_4, \tag{1}$$

$$2Co_3O_4 + 6Sm_2O_3 \rightarrow 6Sm_2CoO_4 + O_2. \tag{2}$$

The above assumption is consistent with the increase in the Sm_2CoO_4 content from 4 wt % in the precursor to 8 wt % after POM (as evaluated by Rietveld method).

The TGA of the composite discharged from the reactor after POM shows a slight weight loss when heated to 100°C, probably due to the removal of water and adsorbed gases, followed by a weight increase, up to 1.95% at 700°C (Fig. 4). This increase may be attributable
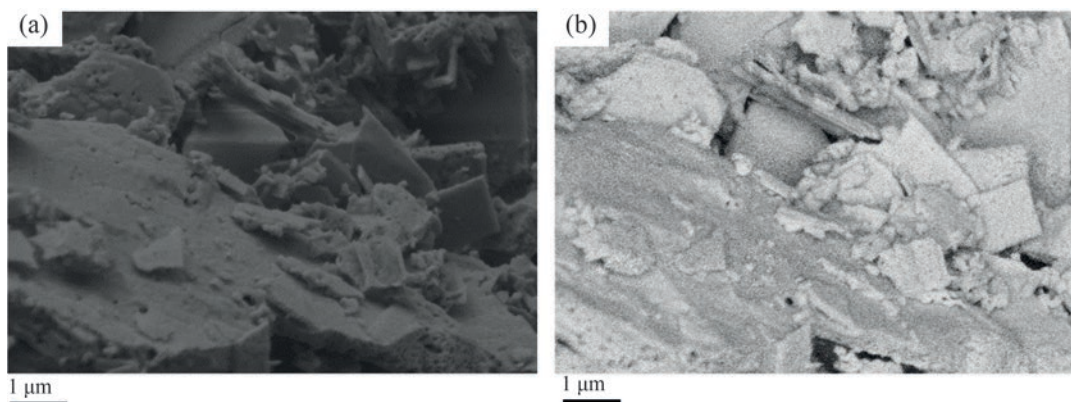

Fig. 2. Micrographs of composite generated from **KtSmCoO** after POM under conditions specified in Table 1: (a) in secondary electrons; and (b) in backscattered electrons.

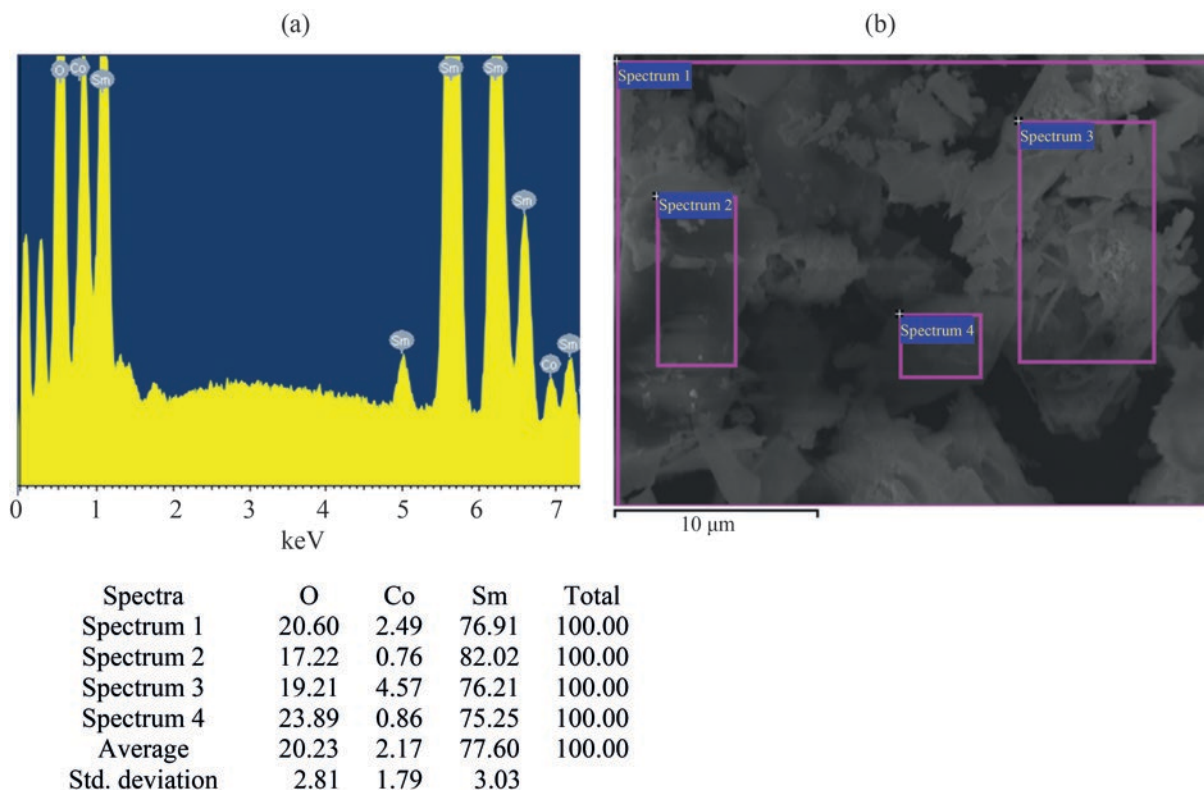| Spectra	O	Co	Sm	Total
Spectrum 1	20.60	2.49	76.91	100.00
Spectrum 2	17.22	0.76	82.02	100.00
Spectrum 3	19.21	4.57	76.21	100.00
Spectrum 4	23.89	0.86	75.25	100.00
Average	20.23	2.17	77.60	100.00
Std. deviation	2.81	1.79	3.03	

Fig. 3. EDX data for **KtSmCoO** catalyst after POM under conditions specified in Table 1: (a) spectrogram with reflections of detected elements; and (b) electronic image of catalyst surface with indication of detection regions.

to reactions (1) and (2) involving metallic cobalt, cobalt oxide, and samarium oxide, and/or to the potential formation of a perovskite by reaction (3):

$$4Co_3O_4 + O_2 + 6Sm_2O_3 \rightarrow 12SmCoO_3. \quad (3)$$
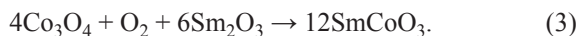
No appreciable weight loss caused by the combustion of carbonaceous deposits was detected.

To reach high yields of syngas in POM more rapidly, another series of experiments was carried out. Here, the **KtSmCoO** catalyst was preheated in hydrogen to 900°C; the catalyst was then reduced at this temperature for 1 h; and a CH_4–O_2 mixture was injected at 12 L g^{-1} h^{-1}. The results are presented in Table 2.

Table 2 clearly shows that the hydrogen prereduction did not improve the POM results. At 900°C it took about 6 h to synthesize a high-performance POM catalyst. Like in the previous series of experiments, further POM occurrence at this temperature enhanced the yields of CO and H_2 to 91%. Likewise, subsequent cooling caused a

predictable decrease in the yields, to 80% at 850°C and to 57% at 800°C.

Cooling the reactor to 750°C likewise rendered the catalyst inactive in POM, with only deep oxidation of methane occurring. Subsequent reheating to 900°C saw the CO and H_2 yields recover to 84–87%, i.e. lower than

Table 2. POM results for KtSmCoO prereduced in hydrogen at 900°C

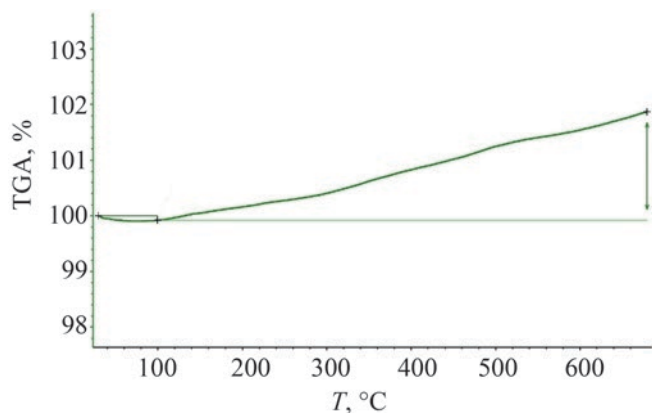| Run no.	Time, min	T, °C	Conversion, %		Yield, %	
			CH_4	O_2	H_2	CO
1	50	900	34	99	4	4
2	355	900	90	99	72	72
3	515	900	98	99	91	91
4	610	850	95	98	80	80
5	710	800	81	99	57	57
6	790	750	40	99	0	0
7	855	900	98	98	84	84
8	1045	900	99	98	87	87
9	1160	900	99	99	84	84

Fig. 4. TGA data for catalyst after POM under conditions specified in Table 1.
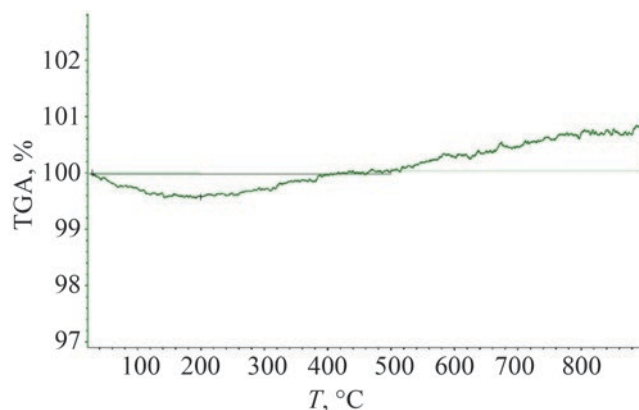

Fig. 5. TGA data for hydrogen-reduced catalyst after POM under conditions specified in Table 2.

in the presence of the non-prereduced catalyst. Thus, the prereduction of **KtSmCoO** in hydrogen did not accelerate the formation of metallic cobalt, an element that must be present to ensure high performance of POM [19, 28].

The XRD powder pattern of the catalyst discharged from the reactor after the above-mentioned series of experiments (Fig. 1, curve *3*) displays a markedly increased (from 4 to 41% by Rietveld method) concentration of Sm_2CoO_4, as well as the formation of $SmCoO_3$ (3% by Rietveld method). The formation of these phases can be explained by the interaction of the metallic cobalt formed during the hydrogen reduction with the feed gas mixture's oxygen and with the excess samarium oxide according to reactions (1)–(3).

Figure 5 illustrates the TGA data for the hydrogen-prereduced **KtSmCoO** after POM under the conditions specified in Table 2. As in the previous POM series, the spent catalyst exhibited some weight loss when heated to 200°C, apparently due to the removal of water and adsorbed gases. Above 400°C, a slight weight increase (0.83%) was observed, likely resulting from reactions (1)–(3) with the nanoparticles of cobalt metal and cobalt oxide being involved (these nanoparticles were missed by XRD). No significant weight loss consistent with the combustion of carbonaceous deposits was observed.

The above discussion proves that the minor decrease in the POM performance of the catalyst in the case of its hydrogen prereduction was associated with some causes other than carbonization. Vella et al. [29], who studied the POM reaction in the presence of a $LaNiO_3$ perovskite,

believe that its low performance was to some extent attributed to the formation of an inactive La_2NiO_4. In our case, the high content of the Sm_2O_3-stabilized Sm_2CoO_4 phase identified in the catalyst after POM may have impaired its performance in a similar manner.

Dry Reforming of Methane

When setting up a series of DRM experiments, we relied on the POM test results described above as well as on the data reported in [25–27]. All these findings suggested that hydrogen prereduction is not a necessary step for the synthesis of a high-performance DRM catalyst. The **KtSmCoO** catalyst was heated to 900°C in an equimolar CH_4–CO_2 mixture flowing to the reactor at a rate of 15 L g^{-1} h^{-1} (Table 3).

Table 3 shows that, as in the POM case, at 900°C the CO and H_2 yields steadily increased, and reached 91 and 90%, respectively, after 6.8 h. As the DRM was continued at 900°C, the yields of CO and H_2 slightly decreased, then were stabilized at 86–88%. Subsequent cooling to 800°C led to a decrease in the yields of CO and H_2, specifically to 60% and 52–54%, respectively. At 700°C, these yields dropped to 12–13% and 7–8%, respectively.

The trends observed under the cooling, specifically the significant formation of water and the CO yields superior to the hydrogen yields, indicate an increasing intensity of the reverse water–gas shift reaction (RWGSR):

$$H_2 + CO_2 \leftrightarrow H_2O + CO. \qquad (4)$$

Table 3. DRM results for KtSmCoO heated to 900°C in reagent mixture

Run no.	Time, min	T, °C	Conversion, %		Yield, %		Run no.	Time, min	T, °C	Conversion, %		Yield, %	
			CH_4	O_2	H_2	CO				CH_4	O_2	H_2	CO
1	10	900	48	64	26	45	11	438	900	89	93	88	87
2	55	900	52	68	36	51	12	508	900	88	94	87	87
3	95	900	60	74	49	62	13	552	900	88	93	87	86
4	145	900	68	80	58	68	14	597	800	59	70	52	60
5	200	900	74	83	69	73	15	612	800	57	69	54	60
6	260	900	78	86	76	78	16	672	700	12	22	8	13
7	305	900	79	88	79	79	17	692	700	12	23	7	12
8	340	900	82	88	79	79	18	762	600	5	7	0	0
9	390	900	83	89	82	80	19	822	900	91	96	91	88
10	408	900	90	96	90	91	20	842	900	91	96	91	88

At 600°C syngas formation completely ceased. Nonetheless, the yields of CO and H_2 regained high levels (88% and 91%, respectively) after reheating to 900°C.

The XRD powder pattern of the post-DRM catalyst (Fig. 1, curve 4) displays intense Sm_2O_3 reflections, the formation of 9 wt % (by Rietveld method) of Sm_2CoO_4, and trace amounts of metallic cobalt. The catalyst was attracted by magnet, thus indicating the presence of metallic cobalt particles too small to be detected by XRD.

The EDX data for the post-DRM sample (Fig. 6) show 2 wt % of cobalt in the catalyst particles, consistent with the Co content in the initially synthesized **KtSmCoO**. This agrees with the assumption that cobalt was largely represented by XRD-undetectable particles.

The TGA data for the composite discharged from the reactor after DRM are illustrated in Fig. 7. The spent catalyst exhibited a minor weight variation not exceeding 0.6 wt %. At temperatures below 350°C, a weight loss
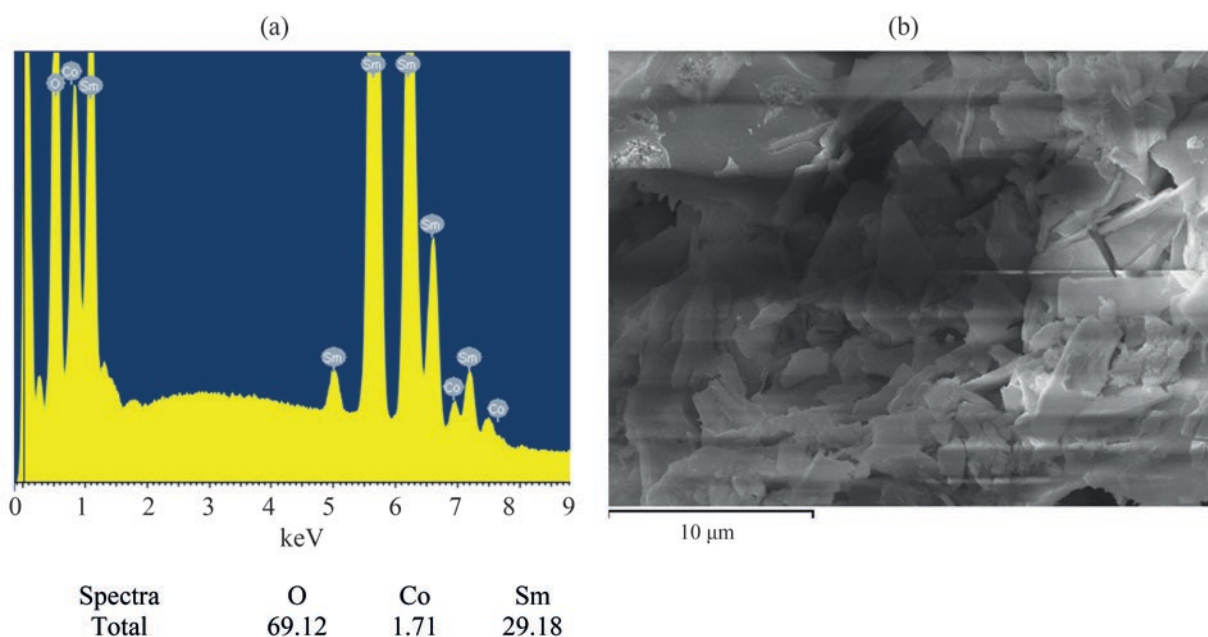

Spectra	O	Co	Sm
Total	69.12	1.71	29.18

Fig. 6. EDX data for **KtSmCoO** catalyst after DRM under conditions specified in Table 3: (a) spectrogram with reflections of detected elements; and (b) electronic image of catalyst surface under detection.
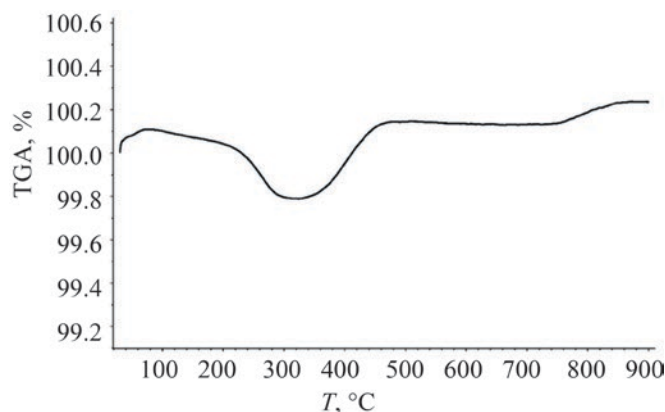
Fig. 7. TGA data for catalyst after DRM under conditions specified in Table 3.

Fig. 8. Micrograph of post-DRM catalyst recorded in secondary electrons.

of 0.32% was observed, apparently due to the removal of adsorbed water and gases. The 0.36% weight increase above 300°C probably resulted from the oxidation of metallic cobalt. Another weight increase, by 0.1% above 700°C, was likely caused by reactions (1)–(3). No weight loss attributable to the combustion of carbonaceous deposits was detected.

Figure 8 provides the SEM micrograph of the catalyst discharged from the reactor after DRM. The image clearly shows a variety of flat (about 200 nm thick) catalyst particles that have pores about 40 nm in diameter; these particles have a non-uniform size distribution. There are no fragments attributable to carbonaceous deposits or fibers.

Previously we synthesized a $SmCoO_3$ catalyst by a similar simplified method and tested it in DRM [24]. The synthesized material contained samarium oxide and cobalt oxide in addition to a $SmCoO_3$ perovskite. Although at 800–900°C this catalyst exhibited near-quantitative yields of syngas, it had 10-fold higher cobalt content than **KtSmCoO** and was prone to major carbonization, potentially threatening to clog the reactor. In [25–27], DRM was carried out in the presence of a catalyst generated from a $SmCoO_3$ perovskite synthesized by the citrate sol–gel method. At 800°C, the conversion of methane and CO_2 was 93%, and the yields of CO and H_2 amounted to 65 and 67%, respectively [25–27]. While the **KtSmCoO** catalyst we prepared at 800°C exhibited similar yields of CO and H_2 (60% and 52-54%, respectively), this was achieved
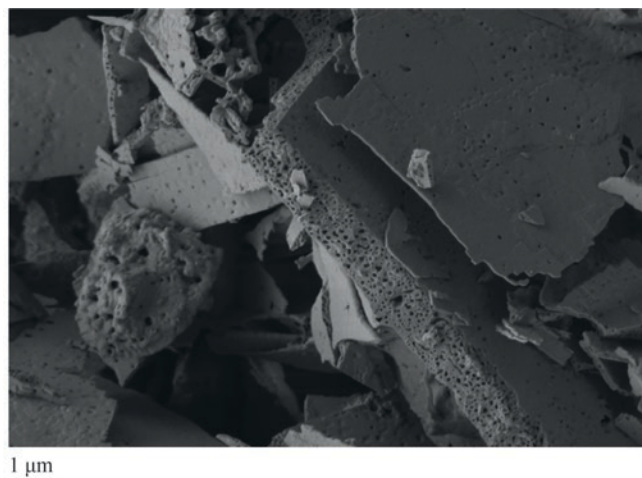
at methane conversion of 57–59% and CO_2 conversion of 69–70%, indicative of higher selectivity. Unlike the $SmCoO_3$ catalysts described in [24–27], our **KtSmCoO**-based catalyst underwent no carbonization in DRM. The CO productivity of the **KtSmCoO**-based catalyst in DRM was 6000 moles per gram-atom of Co per hour (mol g-at^{-1} h^{-1}) at 800°C and 8658 mol g-at^{-1} h^{-1} at 900°C. The hydrogen productivity was 5400 mol g-at^{-1} h^{-1} at 800°C and 8373 mol g-at^{-1} h^{-1} at 900°C. It is worth noting that the $SmCoO_3$ catalyst prepared by the similar method in [24] proved to be noticeably less productive in DRM. Its CO productivity was 762 and 855 mol g-at^{-1} h^{-1} at 800°C and 900°C, respectively, and its hydrogen productivity was 762 and 864 mol g-at^{-1} h^{-1} at 800°C and 900°C, respectively. The single-phase $SmCoO_3$ perovskite described in [25–27] exhibited CO and hydrogen productivity as low as 231 mol g-at^{-1} h^{-1} at 800°C.

Thus, the **KtSmCoO**-based DRM catalyst was not only resistant to carbonization, but showed high syngas productivity per gram-atom of Co contained therein.

CONCLUSIONS

A novel carbonization-resistant catalyst for POM and DRM was prepared. The initially synthesized **KtSmCoO** material containing 2 wt% Co was shown to consist of samarium oxide and Sm_2CoO_4.

The catalyst generated from **KtSmCoO** in situ during POM achieved syngas yields of 63% at 800°C and 93–94% at 900°C. The in situ POM catalyst exhibited

higher performance than its counterpart prepared by the hydrogen prereduction of **KtSmCoO**.

In DRM, the catalyst generated in situ from **KtSmCoO** demonstrated markedly higher syngas productivity per gram-atom of cobalt contained therein than its previously known counterparts. The syngas yields were 50–60% at 800°C and 88–90% at 900°C. A major advantage of the novel catalyst is zero carbonization, both in POM and DRM. The approach developed in this study for the preparation of carbonization-resistant POM and DRM catalysts is also applicable to materials based on other rare-earth elements.

AUTHOR INFORMATION

A.S. Loktev, ORCID: https://orcid.org/0000-0002-5841-8085

V.A. Arkhipova, ORCID: https://orcid.org/0000-0002-2751-4840

M.A. Bykov, ORCID: https://orcid.org/0000-0002-5000-9199

A.A. Sadovnikov, ORCID: https://orcid.org/0000-0002-3574-0039

A.G. Dedov, ORCID: https://orcid.org/0000-0001-8086-2345

ACKNOWLEDGMENTS

FUNDING

CONFLICT OF INTEREST

The authors declare no conflict of interest requiring disclosure in this article.

OPEN ACCESS

REFERENCES

1. Rostrup-Nielsen, J.R., *Catal. Today*, 2002, vol. 71, nos. 3–4, pp. 243–247.
https://doi.org/10.1016/S0920-5861(01)00454-0

2. Liu, K., Song, C., and Subramani, V., *Hydrogen and Syngas Production and Purification Technologies*, Wiley-Interscience, 2009.

3. Hu, Y.H. and Ruckenstein, E., *Adv. Catal.*, 2004, vol. 48, pp. 297–345.
https://doi.org/10.1016/S0360-0564(04)48004-3

4. Enger, B.C., Lødeng, R., and Holmen, A., *App. Catal. A: General*, 2008, vol. 346, nos. 1–2, pp. 1–27.
https://doi.org/10.1016/j.apcata.2008.05.018

5. Moiseev, I.I., Loktev, A.S., Shlyakhtin, O.A., Mazo, G.N., and Dedov, A.G., *Petrol. Chem.*, 2019, vol. 59, no. 1, pp. S1–S20.
https://doi.org/10.1134/S0965544119130115

6. Ranjekar, A.M. and Yadav, G.D., *J. Indian Chem. Soc.*, 2021, vol. 98, p. 100002.
https://doi.org/10.1016/j.jics.2021.100002

7. Bhattar, S., Abedin, Md.A., Kanitkar, S., and Spivey, J.J., *Catal. Today*, 2021, vol. 365, pp. 2–23.
https://doi.org/10.1016/j.cattod.2020.10.041.

8. Zhenghong, B. and Fei, Y., *Adv. Bioenerg.*, 2018, vol. 3, pp. 43–76.
https://doi.org/10.1016/bs.aibe.2018.02.002

9. Kang, J.S., Kim, D.H., Lee, S.D., Hong, S.I., and Moon, D.J., *App. Catal. A: General*, 2007, vol. 332, no. 1, pp. 153–158.
https://doi.org/10.1016/j.apcata.2007.08.017

10. Song, C.S. and Wei, P., *Catal. Today*, 2004, vol. 98, no. 4, pp. 463–484.
https://doi.org/10.1016/j.cattod.2004.09.054

11. Pena, M.A., Gomez, J.P., and Fierro, J.L.G., *App. Catal. A: General*, 1996, vol. 144, pp. 7–57.

12. Al-Sayari, S.A., *Open Catal. J.*, 2013, vol. 6, pp. 17–28.
https://doi.org/10.2174/1876214X20130729001

13. Yin, X. and Hong, L., *App. Catal. A: General*, 2009, vol. 371, nos. 1–2, pp. 153–160.
https://doi.org/10.1016/j.apcata.2009.09.044

14. Choudhary, V.R., Mondal, K.C., Mamman, A.S., and Joshi, U.A., *Catal. Lett.*, 2005, vol. 100, nos. 3–4, pp. 271–276.
https://doi.org/10.1007/s10562-004-3467-0

15. Silva, C.R.B., da Conceição, L., Ribeiro, N.F.P., and Souza, M.M.V.M.., *Catal. Commun.*, 2011, vol. 12, no. 7, pp. 665–668.
https://doi.org/10.1016/j.catcom.2010.12.025

16. Morales, M., Espiell, F., and Segarra, M., *Int. J. Hydrogen Energy*, 2014, vol. 39, no. 12, pp. 6454–6461.
https://doi.org/10.1016/j.ijhydene.2014.02.060

17. Guo, C., Zhang, X., Zhang, J., and Wang, Y., *J. Mol. Catal. A: Chemical*, 2007, vol. 269, nos. 1–2, pp. 254–259.
https://doi.org/10.1016/j.molcata.2007.01.029

18. Peña, M.A. and Fierro, J.L.G., *Chem. Rev.*, 2001, vol. 101, no. 7, pp. 1981–2018.
https://doi.org/10.1021/cr980129f

19. Lago, R., Bini, G., Peña, M.A., and Fierro, J.L.G., *J. Catal.*, 1997, vol. 167, no. 1, pp. 198–209.
https://doi.org/10.1006/jcat.1997.1580

20. Elbadawi, A.H., Ge, L., Li, Z., Liu, S., Wang, S., and Zhu, Z., *Catal. Rev.*, 2021, vol. 63, no. 1, pp. 1–67.
https://doi.org/10.1080/01614940.2020.1743420

21. Royer, S., Duprez, D., Can, F., Courtois, X., Batiot-Dupeyrat, C., Laassiri, S., and Alamdari, H., *Chem. Rev.*, 2014, vol. 114, no. 20, pp. 10292-10368.
https://doi.org/10.1021/cr500032a

22. Zhu, H., Zhang, P., and Dai, S., *ACS Catal.*, 2015, vol. 5, no. 11, pp. 6370–6385.
https://doi.org/10.1021/acscatal.5b01667

23. Dedov, A.G., Loktev, A.S., Ivanov, V.K., Bykov, M.A., Mukhin, I.E., Lidzhiev, M.M., Rogaleva, E.V., and Moiseev, I.I., *Dokl. Phys. Chem.*, 2015, vol. 461, no. 2, pp. 73–79.
https://doi.org/10.1134/S0012501615040028

24. Loktev, A.S., Mukhin, I.E., Bykov, M.A., Sadovnikov, A.A., Osipov, A.K., and Dedov, A.G., *Petrol. Chem.*, 2022, vol. 62, pp. 526–543.
https://doi.org/10.1134/S0965544122020207

25. Osazuwa, O.U., Setiabudi, H.D., Rasid, R.A., and Cheng, C.K., *J. Natur. Gas Sci. Eng.*, 2017, vol. 37, pp. 435–448.
https://doi.org/10.1016/j.jngse.2016.11.060

26. Osazuwa, O.U. and Cheng, C.K., *J. Clean. Product.*, 2017, vol. 148, pp. 202–211.
https://doi.org/10.1016/j.jclepro.2017.01.177

27. Osazuwa, O.U. and Cheng, C.K., *Malaysian J. Catal.*, 2017, vol. 2, pp. 12–17.

28. Toniolo, F.S., Newton, R., Magalhaes, S.H., Perez, C.A.C., and Schmal, M., *Appl. Catal. B: Environmental*, 2012, vols. 117–118, pp. 156–66.
https://doi.org/10.1016/j.apcatb.2012.01.009

29. Vella, L.D., Villoria, J.A., Specchia, S., Mota, N., Fierro, J.L.G., and Specchia, V., *Catal. Today*, 2011, vol. 171, pp. 84–96.
https://doi.org/10.1016/j.cattod.2011.03.074

30. Dedov, A.G., Loktev, A.S., Komissarenko, D.A., Mazo, G.N., Shlyakhtin, O.A., Parkhomenko, K.V., Kiennemann, A.A., Roger, A.-C., Ishmurzin, A.V., and Moiseev, I.I., *Appl. Catal. A: General*, 2015, vol. 489, pp. 140–146.
https://doi.org/10.1016/j.apcata.2014.10.027

31. Zagaynov, I.V., Loktev, A.S., Arashanova, A.L., Kutsev, S.V., Ivanov, V.K., Dedov, A.G., and Moiseev, I.I., *Chem. Eng. J.*, 2016, vol. 290, pp. 193–200.
https://doi.org/10.1016/j.cej.2016.01.066

32. Rietveld, H.M., *J. Appl. Crystallogr.*, 1969, vol. 2, pp. 65–71.
https://doi.org/10.1107/S0021889869006558